Very High Cycle Corrosion Fatigue Study of the Collapsed Polcevera Bridge, Italy

Stefano Invernizzi[1]; Francesco Montagnoli[2]; and Alberto Carpinteri, F.ASCE[3]

Abstract: A possible scenario is proposed to put into evidence how the combined effect of fatigue at very high number of cycles and corrosion could have been responsible for the failure of one of the strands and the subsequent collapse of the so-called balanced system of the Polcevera Bridge designed by Morandi. The analysis accounts for an actual estimation of the heavy-lorry traffic and load spectrum, as well as for the European Standards prescription for the fatigue damage accumulation assessment. In addition, the effective construction phases of the viaduct are considered. The structural analysis is carried out by means of analytical models, in order to simplify the structure complexity without prejudice to the description of the most relevant aspects of the structural behavior. The main purpose is to warn the scientific community and the public administrations that the combined effects of low-amplitude fatigue and corrosion can be dangerously underestimated, and that the existing assets of 20th century bridges deserve special attention in this respect. **DOI: 10.1061/(ASCE)BE.1943-5592.0001807**.

Introduction

The present European Standards concerning fatigue assessment in bridges prescribe to adopt the stress-life approach, and to refer to a bounded Wöhler's curve with cut-off in correspondence of 10^8 cycles (Nussbaumer et al. 2018). Although the existence of the fatigue limit is still controversial (Bathias and Paris 2004), this approach looks reasonable, at least when degradation is avoided and when the load spectrum due to heavy traffic has been estimated correctly (CEN 2003). The standards also provide methods for the correct estimation of the load spectrum (CEN 2003), together with prescriptions regarding the limitation to degradation, the monitoring of steel tendons, and the possibility of replacement of degraded elements. The picture is different if existing bridges are considered. In particular, in the case of 20th century bridges, the corrosion of metallic parts can be developed more than expected due to both poor maintenance and underestimation of the aggressiveness of the environment. At the same time, the load spectrum has dramatically increased in terms of relative and absolute frequency of heavy lorries. As a consequence, there is a consistent number of bridges that should be assessed with respect to very high cycle fatigue (VHCF) phenomena, because they have already overcome more than 10^8 cycles, or will exceed them soon in the next few decades. The corrosion of steel elements subjected to cyclic loading in an aggressive environment is known as corrosion fatigue (Perez-Mora et al. 2015), and the resulting effects include both the reduction in the resisting cross-section and the downwards translation of Wöhler's curve together with the vanishing of the fatigue limit. When the aggressive environment is combined with poor maintenance and VHCF, the phenomena interact reducing the safety margin of the structure much more quickly than expected. The Polcevera viaduct (Genoa, Italy), a renowned cable-stayed concrete bridge designed by Morandi (1968) some five decades ago and partially collapsed on the August 14, 2018 (Fig. 1), is taken as case study to show that the effect of corrosion fatigue on existing historical bridges deserves more attention.

The old viaduct has been completely dismantled and replaced by a new one, which was opened to traffic on August 3, 2020.

As shown in the following, the cross-section of the cable-stay close to the antenna is the most critical. This hypothesis is consistent with the image shown in Fig. 2(a), which was taken from a recently declassified video, where it is possible to appreciate the very first instants of the collapse. First, the cross-section close to the antenna of the South-East (SE) cable-stay suddenly broke apart (A). Then the bridge-deck and the adjacent Gerber beam (on the right) collapsed (B). At the same time, due to dynamic rebound and missing balance, the top of the antenna broke and rotated anticlockwise (C). The rebound was such that the cable-stay on the left side buckled in compression (D), propagating the failure to the left side of the bridge deck and Gerber beam (E). A key role in the collapse was certainly played by corrosion. Fig. 2(b) shows part of the corroded tendons that were considered in the forensic analysis.

Although forensic investigation is still under development, and without any claim to provide the ultimate interpretation for the failure, a simplified structural model is presented, which allows for the determination of the mean stress in the strands. The fatigue load spectrum is obtained based on the line of influence of the stay cable axial force traced for vertical loads moving along the bridge deck and considering some relevant information about the lorries' statistics. The accumulation of damage is calculated according to the Miner approach, with reference to different scenarios. In the following, the mechanical behavior of the cable-stay is considered in detail. Although simple analytical models are used, the complex construction phases of the stay, the geometrical nonlinearities of the cables, the stress losses due to prestressing of the concrete covering of the steel tendons, and the mechanism of stress redistribution

[1]Dept. of Structural, Geotechnical and Building Engineering, Politecnico di Torino, Corso Duca degli Abruzzi 24, 10129 Torino, Italy (corresponding author). ORCID: https://orcid.org/0000-0001-6334-7931. Email: stefano.invernizzi@polito.it

[2]Dept. of Structural, Geotechnical and Building Engineering, Politecnico di Torino, Corso Duca degli Abruzzi 24, 10129 Torino, Italy. Email: francesco.montagnoli@polito.it

[3]Dept. of Structural, Geotechnical and Building Engineering, Politecnico di Torino, Corso Duca degli Abruzzi 24, 10129 Torino, Italy; Dept. of Civil and Environmental Engineering, Shantou Univ., Shantou 515063, China. Email: alberto.carpinteri@polito.it

Note. This manuscript was submitted on January 26, 2021; approved on September 10, 2021; published online on November 15, 2021. Discussion period open until April 15, 2022; separate discussions must be submitted for individual papers. This paper is part of the ***Journal of Bridge Engineering***, © ASCE, ISSN 1084-0702.

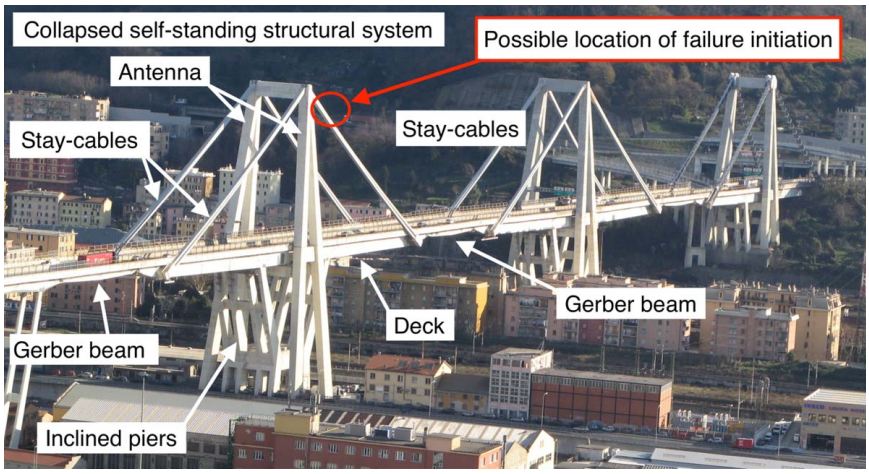

Fig. 1. Three self-standing structural systems of the Morandi Bridge, with details of the structural elements and possible location of initial failure. (Image courtesy of Wikimedia Commons/Bubici Paolo.)

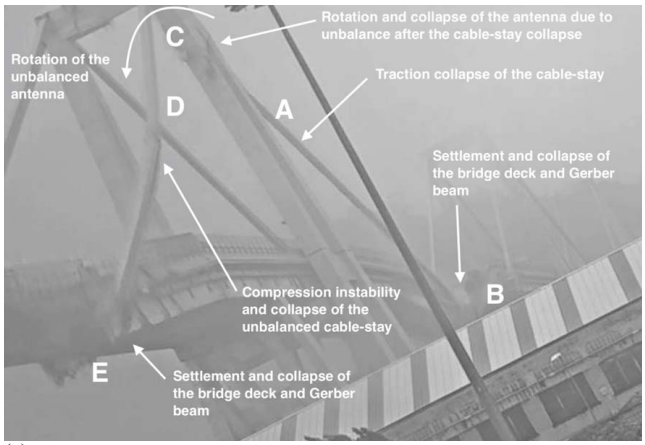

(a)

(b)

Fig. 2. (a) Triggering of the bridge collapse, which started from the failure of the SE cable-stay cross-section close to the antenna (image courtesy of Guardia di Finanza di Genova 2019); and (b) picture of the corroded strands subjected to forensic analysis (image courtesy of Polizia di Stato, republished from Bonchi (2020) with permission from Genova24).

due to the degradation and corrosion evolution will all be considered. In this way, not only will the consistency of the decompression hypothesis be proven, but it will also be shown that the cable-stay could have retained almost its initial stiffness up to the moment of failure, therefore resulting in a very brittle condition.

The Morandi Bridge Conception and Construction

Morandi (1968) conceived the design of the viaduct above the Polcevera river in order to minimize the interference with the existing railways and buildings adopting, for the three main spans, the so-called self-standing structural system. The first construction phase concerned the erection of the A shaped piles ("antennas") and of the inclined support pillars. After this stage, the construction of the bridge deck began, proceeding by casting the deck segments in both directions symmetrically with respect to the pile. The use of extensive scaffolding structures was avoided thanks to temporary tendons placed at some distance above the deck to increase the internal lever arm, as shown in Fig. 3(a). Once the hanging points for the cable-stays were reached, and the construction of the antenna finalized, the positioning of the inner tendons began. The progressive tensioning of the inner tendons proceeded together with the removal of the temporary tendons, always taking care to keep the vertical displacement of the hanging point equal to zero. This initial phase of construction of the cable-stay will be referred to in the following as *phase 1*. Thereafter, the two transverse connection beams were cast, and the last hanging sections of the deck launched. Another very peculiar aspect of the Morandi conception was the idea to replace the ordinary steel cable-stays with prestressed reinforced concrete ones. The objective was twofold: first, to provide protection against steel corrosion of the cables exploiting the concrete covering; and, second, to drastically increase the axial stiffness of the cable-stays. The concrete covering could not be realized in only one solution, because the change of geometry of the inner tendon catenary could not be sustained by concrete without severe cracking. Therefore, the covering was first cast in segments [Fig. 3(b)] that could allow the displacement of the catenary without damage (*phase 2*). After the curing, the joints among segments were filled and external strands were placed in the ducts and prestressed in order to guarantee compression stress state in the concrete covering (*phase 3*). Finally, the ducts were injected and the extremities of the external strands connected to the transverse beam. The construction of the three self-sustained systems could proceed at the same time, minimizing the duration of the building site. The placing of the Gerber beams between the self-standing systems (*phase 4*), according to the photographic documentation, took place during or immediately after the construction of the concrete covering, dependent on the considered self-standing system. One relevant advantage of the Morandi structural conception was that the variable

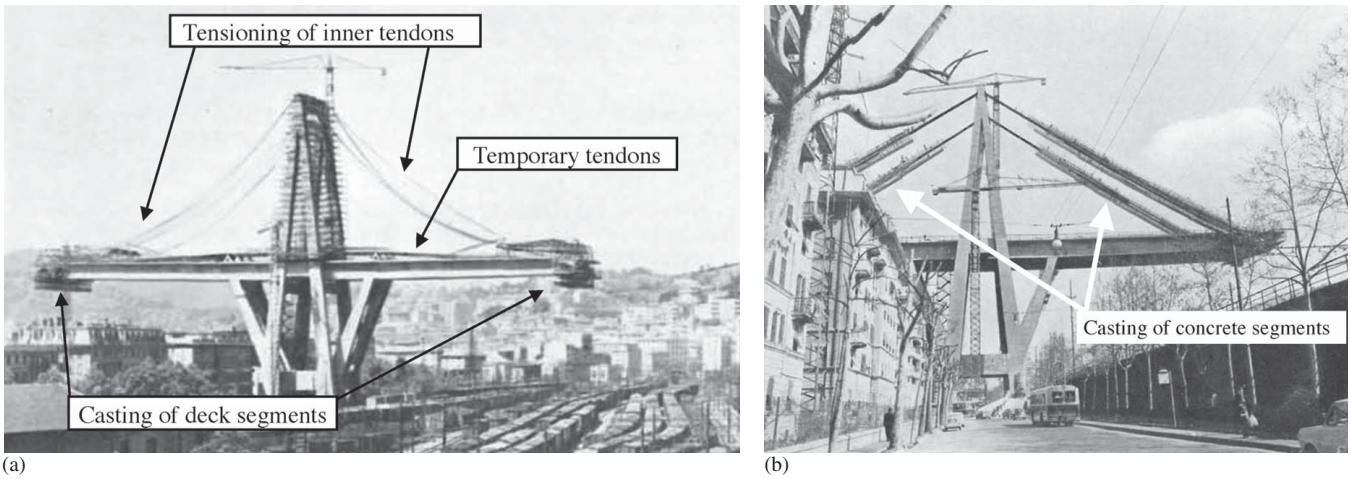

Fig. 3. Construction phases: (a) sequential casting of deck segments; and (b) progressive casting of the concrete covering segments around the cable-stays. [Reprinted from Morandi (1968), under Creative Commons-BY-4.0 (https://creativecommons.org/licenses/by/4.0/).]

loads (*phase 5*) would have been carried by the whole homogenized concrete cross-section of the cable-stays, in place of the steel tendons alone, providing very limited oscillating stresses.

Analytical Structural Model

A few studies can be found in the literature concerning the structural behavior of the collapsed self-standing system, all of them involving very complex finite element or discrete element calculations. These analyses were able to provide, starting from the assumption of a weak section, the kinematics of the collapse with great details. In contrast, they were quite ineffective in describing the possible mechanism that was at the origin of the failure mechanism. Alternatively, a simplified analytical model can be exploited to gain more insight about the damage accumulation. The Polcevera bridge was composed of several statically determinate Gerber beams of 36 m span each and three main self-standing structural systems. Each balanced system designed by Morandi was a quite complicated structure itself and it is worth, as a first step, limiting the analysis to the bridge deck. The deck of the self-sustained system was a multicell box girder 4.5 m deep and 18 m wide (Fig. 4), which was supported at four points by inclined piers and two couples of stay cables hung at the top of the A-shaped antenna. The link of the deck with the piers and the stay cables is guaranteed by four transverse beams. In other words, each self-standing structural system is a three-span continuous beam with two terminal cantilever beams, which sustain the two lateral simply supported beams by means of Gerber saddles (Fig. 5). Therefore, in order to simplify the analysis and better understand the failure mechanism, our attention has been focused exclusively on the self-standing structural system, which collapsed independently of the remaining parts of the viaduct. Furthermore, for each self-standing structural system, two main substructures can be considered: the first is the deck of Polcevera bridge; the second is made up by the two couples of stays. Therefore, in the following subsection, a detailed analysis of the two main substructures is proposed in order to assess the internal reactions and the corresponding stresses in the deck and, in particular, in the stays.

Static Analysis of the Bridge Deck

According to Morandi's design concept (Morandi 1967), the 352 inner tendons were supposed to support the permanent loads. Thus, the stress in the inner tendons was set, such as the vertical

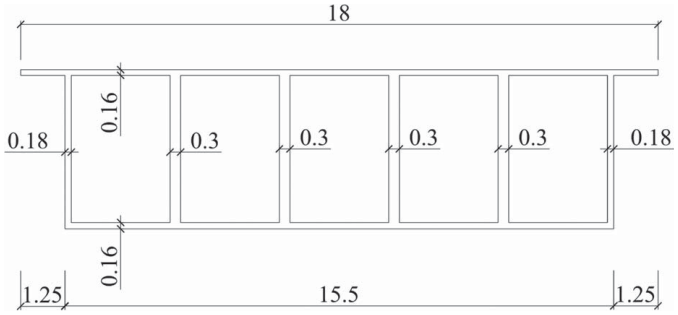

Fig. 4. Cross-sections of the deck.

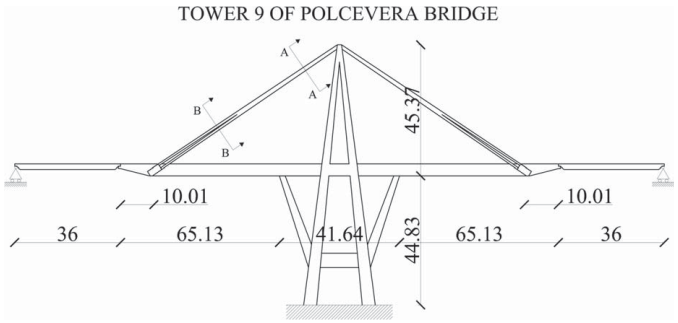

Fig. 5. Lateral view of the self-standing system.

displacement of the deck at the connection point with the stay cables would vanish. As a consequence, the static scheme shown in Fig. 6(a) allows for an easy determination of the axial force in the two couples of stay cables due to the permanent loads (Invernizzi et al. 2019, 2020b). In fact, the axial force in the cable-stays at the connection with the deck can be estimated with no special efforts, given that the cross-section of the main deck is assumed constant, and considering that the 352 steel strands, which were put in place, were continuously retensioned during the removal of provisional tendons (Morandi 1967), in order to vanish the vertical displacement of the hanging section [point A in Fig. 6(a)]. At the same time, the internal actions in the deck can be assessed due to itself self-weight [Fig. 6(b)].

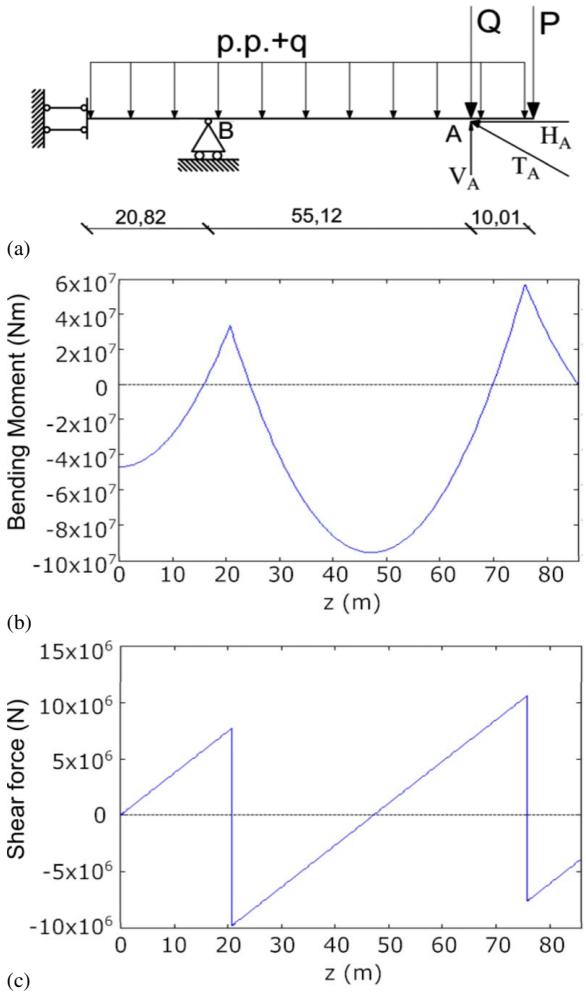

Fig. 6. (a) Simplified static scheme of the right half of the bridge deck; (b) bending moment; and (c) shear force in the deck.

Stress Field in the Post-Tensioned Concrete Stay

In order to evaluate the fatigue damage accumulation in the stay, it is crucial to our purpose to obtain the cable-stay geometry and distribution of stresses with sufficient detail and high-precision (Invernizzi et al. 2020a). This can be achieved exploiting the analytical solution for the elastic catenary (Irwine 1981), with respect to the different construction phases of the cable-stay. In addition, a simple but effective model is introduced in the following to allow for the determination of the state of stress in the cross-section, even in the case of corrosion of the steel strands.

The elastic catenary scheme is represented in Fig. 7, whereas the parametric solution of the deformed elastic line and of the axial force, as a function of the curvilinear coordinate s, are given by the following equations:

$$x(s) = \frac{H}{EA_0}s + \frac{HL_0}{W}\left[\sinh^{-1}\left(\frac{V}{H}\right) - \sinh^{-1}\left(\frac{V - Ws/L_0}{H}\right)\right] \quad (1)$$

$$y(s) = \frac{W}{EA_0}s\left(\frac{V}{W} - \frac{s}{2L_0}\right) + \frac{HL_0}{W}\left[\sqrt{1 + \left(\frac{V}{H}\right)^2} - \sqrt{1 + \left(\frac{V - Ws/L_0}{H}\right)^2}\right] \quad (2)$$

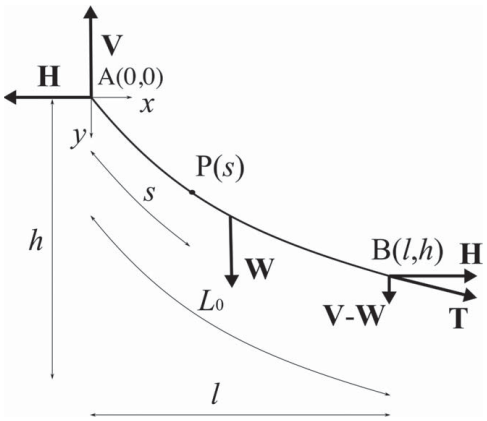

Fig. 7. Structural scheme for the elastic catenary problem.

$$T(s) = \sqrt{H^2 + \left(V - \frac{Ws}{L_0}\right)^2} \quad (3)$$

According to the construction phases, at the end of phase 1, the 352 inner steel strands (Fig. 8) hung at the top of the antenna were set up to constrain the vertical displacement of the deck in correspondence of the transverse girder beam [point A in Fig. 6(a)].

Therefore, the kinematic boundary conditions for the elastic catenary equation are known at both extremities of the cable, whereas the vertical component V–W of the axial force is known at the lower end of the cable, because it must be equal to the vertical reaction at point A [Fig. 6(a)] obtained from the previous analysis of the deck. It is, thus, possible to assume the initial length of the cable L_0 and the horizontal component H of the reaction of axial force T as unknown discrete parameters, to be obtained by solving the corresponding nonlinear algebraic system (Irwine 1981). Those values can be finally substituted into the general solutions [Eqs. (1)–(3)] that provide both the axial force diagram, $T^{(1)}(s)$, and the elastic line as functions of the curvilinear coordinate, s, at the end of phase 1 (Fig. 9, thick continuous line). Therefore, the normal stress in the cross-section of the 352 inner strands, $A_{\text{inn\_st}}$, at the end of phase 1 is calculated as follows:

$$\sigma^{(1)}_{\text{inn\_st}} = \frac{T^{(1)}(s)}{A_{\text{inn\_st}}} \quad (4)$$

At the second stage of the cable-stay construction (phase 2), the concrete covering was cast in several distinct segments in order to allow for the sensible change of the elastic line without cracking of the concrete. In this phase, the concrete segments act as an external load on the 352 inner steel tendons, without providing effective bending stiffness to the cable-stay. The new elastic line can thus be obtained again by solving the catenary equation, simply accounting for the increased dead weight per unit length of the cable due to both the self-weight of the inner steel strands and of the concrete segments. The elastic line of phase 2 is shown in Fig. 9 with a dotted line. Fig. 10 shows the normal stress in the steel strands depending on the considered construction phase , which are given by the following equation:

$$\sigma^{(2)}_{\text{inn\_st}} = \frac{T^{(2)}(s)}{A_{\text{inn\_st}}} \quad (5)$$

where $T^{(2)}(s)$ is the axial force at the end of phase 2. This mechanical quantity is assessed according to (3), once that the horizontal force H and L_0 have been calculated by the Eqs. (1) and (2)

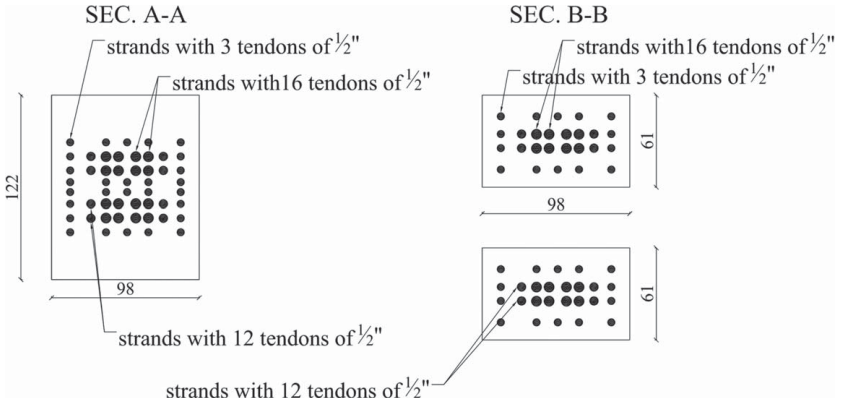

Fig. 8. Cross-section of the stay.

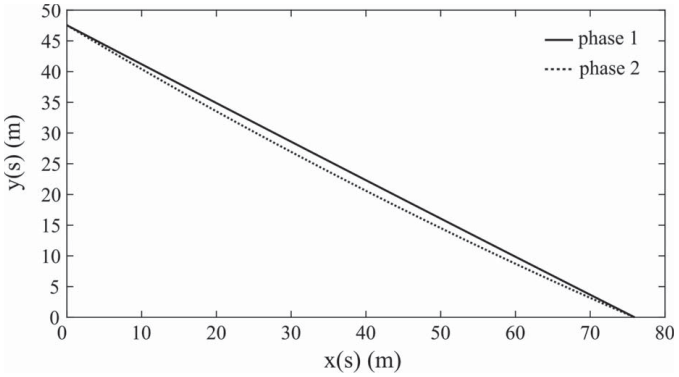

Fig. 9. Deformed configuration of the cable: 352 inner steel strands only (phase 1) and after the casting of the concrete segments (phase 2).

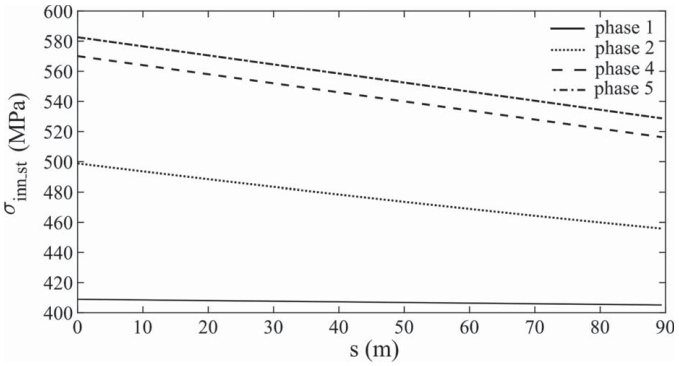

Fig. 10. Variation of the normal stresses in the inner tendons during the different construction phases.

by considering the self-weight of the concrete covering and the inner tendons.

After curing of the concrete segments and filling of the joints, the 112 outer tendons were added and prestressed to provide a negative stress state to the concrete covering and ensuring protection of the steel elements against aggressive environment (phase 3).

During post-tensioning, the outer strands are looped over the top of the antenna, and equal pretensioning is provided in correspondence to the transverse girder beam at the bridge deck. The strands are disposed symmetrically with respect to the cable-stay cross-section. The post-tensioning of the concrete covering does not affect the elastic line configuration because the contraction of the concrete can take place independently of the inner tendons because the relative axial displacement are not yet constrained, so that the normal stress in the inner strands is not affected by the concrete pretensioning:

$$\sigma^{(3)}_{\text{inn\_st}} = \sigma^{(2)}_{\text{inn\_st}} \tag{6}$$

In Table 1 the principal mechanical properties of the construction materials used to make the stay-cables, such as the elastic modulus, the characteristic ultimate tensile strength, and the characteristic compression strength of steel tendons and concrete, are reported.

On the other hand, the stress state of the outer tendons is not uniform nor constant with time. The stress losses due to relaxation and friction along the curved axis of the cable-stay can be assessed according to the European Standards (CEN 2011). The initial pulling stress of 1,200 MPa at the bridge deck connection (Morandi 1967), $\sigma_{p\_0\_\max}$, is thus reduced to 900 MPa due to long-term phenomena. In addition, the prestress losses due to friction can be assessed, being known as the curvature of the elastic line in phase 2. Therefore, the tensile stress in the prestressing outer tendons can be evaluated as follows:

$$\sigma^{(3)}_{\text{out\_st}} = \sigma_{p0}(s) - \Delta\sigma_{p,c+s+r}(s) \tag{7}$$

The term $\sigma_{p\_0}(s)$ is the prestressing stress along the curvilinear coordinate by considering the friction loss, whereas $\Delta\sigma_{p,c+s+r}(s)$ takes into account the stress losses due to the long-term phenomena, that is, creep and shrinkage of concrete and the relaxation of steel tendons. The negative stress state induced in the concrete covering can be calculated, for each section of the cable state, thanks to the compatibility equation for deformation, namely:

$$\sigma^{(3)}_{c} = \sigma^{(3)}_{\text{out\_st}}(s)\frac{A_{\text{out\_st}}}{A_c} \tag{8}$$

where $A_{\text{out\_st}}$ is the cross-section area of the outer tendons, whereas A_c is the reacting cross-section area of the concrete covering.

After post-tensioning of the outer strands, the ducts containing the tendons were injected, and the 112 tendons were linked to the transverse beams of the deck. From this stage on (phase 3) the cable-stay performed as a unique solid prestressed concrete element.

Subsequently, the Gerber beams were put in place,as well as New Jersey barriers, and the flexible road pavement was made (phase 4). At the end of this stage, the normal stress in the three resisting elements is given by the following expressions:

$$\sigma^{(4)}_{\text{inn\_st}} = \sigma^{(3)}_{\text{inn\_st}} + n\frac{\Delta T_{\text{dl}}}{A_{\text{equi\_}c}} \tag{9a}$$

Table 1. Principal mechanical properties of the construction materials used to make the stay-cables

Material	Elastic modulus (MPa)	Ultimate tensile strength (MPa)	Compressive strength (MPa)
Prestressing steel	195,000	1,700	—
Concrete	35,000	—	35

$$\sigma_{\text{out\_st}}^{(4)} = \sigma_{\text{out\_st}}^{(3)} + n\frac{\Delta T_{\text{dl}}}{A_{\text{equi\_}c}} \tag{9b}$$

$$\sigma_{c}^{(4)} = \sigma_{c}^{(3)} + \frac{\Delta T_{\text{dl}}}{A_{\text{equi\_}c}} \tag{9c}$$

where ΔT_{dl} is the increment in the axial force of the stay cable due to the dead load, the term $A_{\text{equi\_}c}$ is the equivalent area of the section in terms of concrete, whereas n is the modular ratio.

The effects of variable loads on the bridge deck is considered in phase 5 according to European Standards (CEN 2003), which are evaluated similarly to what has been done above, that is,

$$\sigma_{\text{inn\_st}}^{(5)} = \sigma_{\text{inn\_st}}^{(4)} + n\frac{\Delta T_{\text{vl}}}{A_{\text{equi\_}c}} \tag{10a}$$

$$\sigma_{\text{out\_st}}^{(5)} = \sigma_{\text{out\_st}}^{(4)} + n\frac{\Delta T_{\text{vl}}}{A_{\text{equi\_}c}} \tag{10b}$$

$$\sigma_{c}^{(5)} = \sigma_{c}^{(4)} + \frac{\Delta T_{\text{vl}}}{A_{\text{equi\_}c}} \tag{10c}$$

where ΔT_{vl} is the increment in the axial force of the stay cable due to the variable load.

It is worth noting that a comparison with the variable loads adopted by Morandi at the design time provided no significant difference as far as the amplitude of the loads is concerned.

Figs. 10–12 show the normal stress in the inner strands, in the outer strands, and in the concrete for the five different construction phases, respectively. It appears evident how the stress losses diminish both the stress level in steel and in the concrete. On the other hand, nonstructural permanent loads increase the level of stress in steel and decrease the absolute value of stress in concrete.

It is worth noting that the structural system conceived by Morandi would have been effective, although not everywhere at the same extent, if only the degradation could be carefully avoided.

Degradation Damage Evaluation of the Stay Cable

In the previous section, it has been shown how the cable-stay conceived by Morandi was able to provide protection against corrosion and high stiffness, in addition to the fact that the variable load cycles were almost completely redistributed to the compressed concrete cross-section of the stays. In this way, the steel fraction of the stay cross-section was practically unaffected by stress oscillations that are at the basis of fatigue damage accumulation phenomena. Unfortunately, at the time of Polcevera bridge construction, the concepts of durability and degradation were not so well-known as nowadays. Even at the end of the 1970s, Morandi was rather worried about the acceleration in the degradation process of the bridge, possibly due to a combination of marine environment and pollution from the nearby steelworks (Morandi 1979).

More recently, some investigations (MIT 2018) have highlighted the nonperfect injection of the ducts with the grout, thus allowing airborne chlorides and sulfides to penetrate inside the ducts and corrode the steel tendons. This degradation process has likely triggered a redistribution of the stresses among concrete and steel of the stays with the consequent decompression of the stays themselves, especially in the region close to the antenna, where the prestressing compression of concrete was less effective.

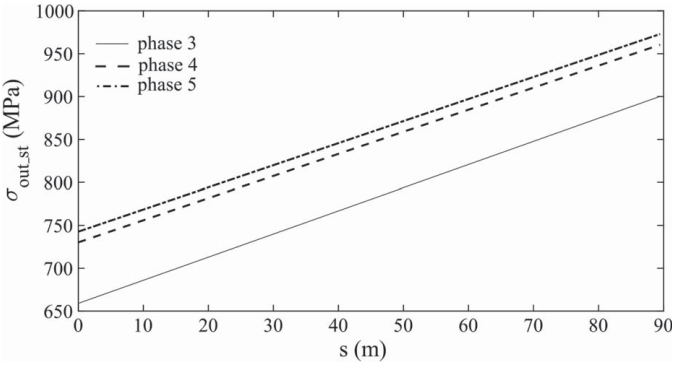

Fig. 11. Variation of the normal stresses in the outer tendons during the different construction phases.

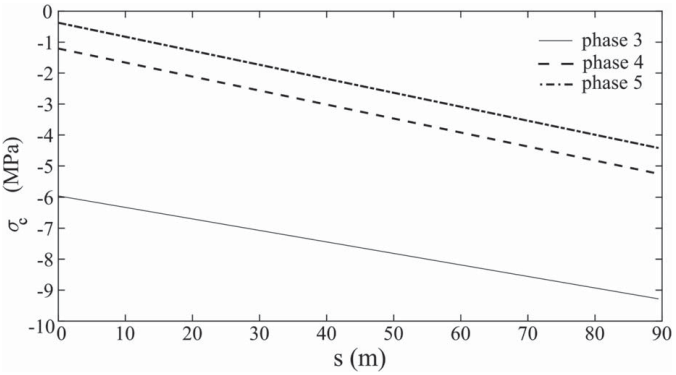

Fig. 12. Variation of the normal stresses in the concrete covering during the different construction phases.

Concrete Covering Decompression

In order to evaluate the effect of corrosion in terms of redistribution of stresses among concrete and steel in the closest section to the antenna, we developed a simple but effective model where the cross-section of the cable-stay (Fig. 8) is schematized by three springs in parallel (Fig. 13), representing the 352 inner strands, the concrete covering, and the 112 outer strands, respectively.

The model provides the overall secant stiffness per unit length of the cable-stay or, in other words, of the cross-section. The calculation is performed increasing step by step the amount of corrosion of the steel tendons. At each step, the model is updated to account for the steel area reduction and the normal stress in each reacting component can be assessed as follows:

$$\sigma_{\text{inn\_st}}(\%C) = \sigma_{\text{inn\_st}}^{(5)} + T(s)\frac{K_{\text{inn\_st}}(\%C)}{K_{\text{tot}}(C\%)} \tag{11a}$$

$$\sigma_{\text{out\_st}}(C\%) = \sigma_{\text{out\_st}}^{(4)} + T(s)\frac{K_{\text{out\_st}}(C\%)}{K_{\text{tot}}(C\%)} \tag{11b}$$

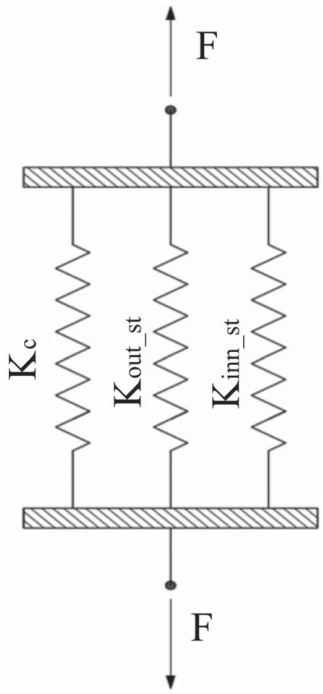

Fig. 13. Simplified structural scheme used to evaluate the unit-length stiffness of the stay cable and redistribution of the normal stresses among the three components.

$$\sigma_c(C\%) = \sigma_c^{(5)} + T(s)\frac{K_c(C\%)}{K_{\text{tot}}(C\%)} \tag{11c}$$

where $K_{\text{inn\_st}}(C\%)$, $K_{\text{out\_st}}(C\%)$, and $K_c(C\%)$ are the secant stiffness per unit length of the inner tendons, the outer tendons, and the concrete covering, respectively, for increasing corrosion level. Moreover, the total cable-stay stiffness, $K_{\text{tot}}(C\%)$, according to the parallel spring scheme (shown in Fig. 13), is the sum of each term.

When the stress in concrete becomes positive, the concrete cross-section and the corresponding stiffness are immediately set to zero. For increasing level of corrosion, when the stress in the steel tendons overcomes the tensile strength, also the steel cross-section and the corresponding stiffness is set to zero. This moment corresponds to the potential failure of the cable-stay under static loading. Therefore, the secant stiffness per unit length of the inner tendons, the outer tendons, and the concrete covering should be assessed in the following way:

$$K_{\text{inn\_st}}(C\%) = \begin{cases} A_{\text{inn\_st}}(C\%)E_s, & \text{if } \sigma_{\text{inn\_st}} < \sigma_u \\ 0, & \text{if } \sigma_{\text{inn\_st}} \geq \sigma_u \end{cases} \tag{12}$$

$$K_{\text{out\_st}}(C\%) = \begin{cases} A_{\text{out\_st}}(C\%)E_s, & \text{if } \sigma_{\text{out\_st}} < \sigma_u \\ 0, & \text{if } \sigma_{\text{out\_st}} \geq \sigma_u \end{cases} \tag{13}$$

$$K_c(C\%) = \begin{cases} A_c E_c, & \text{if } \sigma_c < 0 \\ 0, & \text{if } \sigma_c \geq \sigma_u \end{cases} \tag{14}$$

Note that, according to the sequence of the construction phases, the cable-stay is not subjected to sensible bending moments, thus its structural behavior is assimilated to a truss element, and each component is subjected to uniform stress and strain conditions. Therefore, the stress field redistribution in the three components can be worked out very easily, once that the axial force in a certain

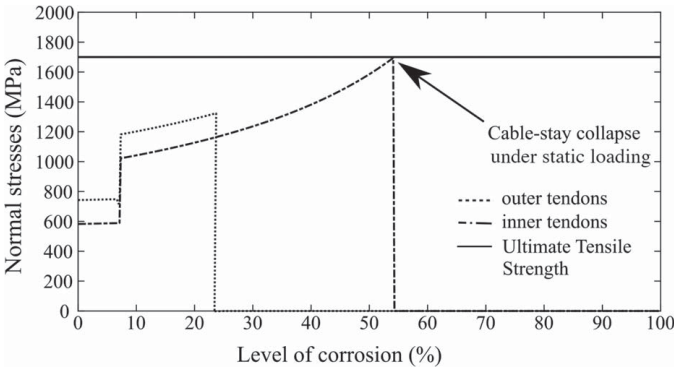

Fig. 14. Variation of the normal stresses in the inner and outer tendons as a function of the corrosion level ($C\%$) for scenario A.

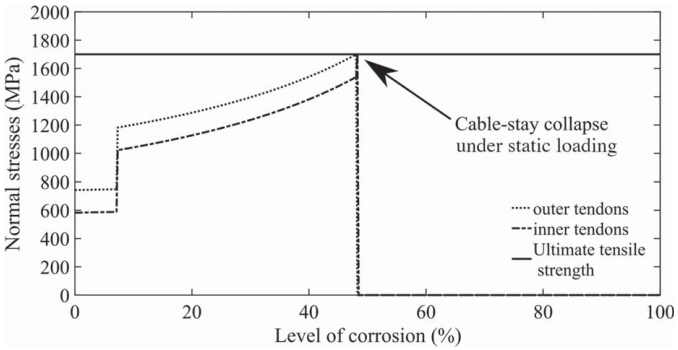

Fig. 15. Variation of the normal stresses in the inner and outer tendons as a function of the corrosion level ($C\%$) for scenario B.

cross-section, together with coaction stresses, are known from the previous calculations. In addition, the adopted parallel spring system implicitly assumes perfect bonding between concrete and steel.

The following three different scenarios are considered (Invernizzi et al. 2020a): *scenario A*, conjecturing that the corrosion progresses starting from the outer strands; *scenario B*, conjecturing that the corrosion advance starting from the inner strands; *scenario C*, conjecturing that the corrosion advances equally both in the inner and outer strands. The analysis is carried out referring to a cross-section close to the antenna (at the origin of the curvilinear abscissa), where the concrete precompression is less effective due to the stress losses in the tendons.

The normal stress variation in the inner and outer tendons are shown, respectively: in Fig. 14 for scenario A; in Fig. 15 for scenario B; and in Fig. 16 for scenario C. In addition, Fig. 17 shows the normal stress variation in concrete, which is identical for the three considered scenarios.

In all the three considered scenarios, in the sections close to the antenna, the concrete decompression occurs with rather low level of corrosion, equal approximately to 7% (Fig. 17). As soon as the concrete decompresses, the concrete area is set equal to zero, the concrete stiffness K_c vanishes, and the redistributed stress σ_c becomes null.

As a consequence, the stress in steel tendons (Figs. 14–16) for each scenario, shows a sudden increase in correspondence of corrosion equal to 7%, both for inner and outer tendons. The discontinuity is followed by gradual increase in stress, due to the progressive reduction of the steel area.

In scenario A (Fig. 14), the cross-section of outer tendons is completely eroded by corrosion progression at a level equal to about 24%. Hence, it is assumed that corrosion proceeds in the

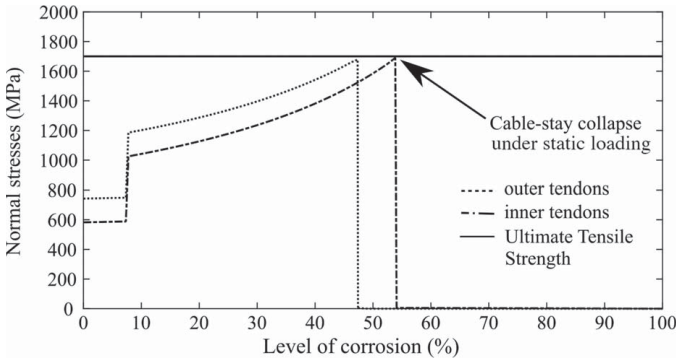

Fig. 16. Variation of the normal stresses in the inner and outer tendons as a function of the corrosion level (C%) for scenario C.

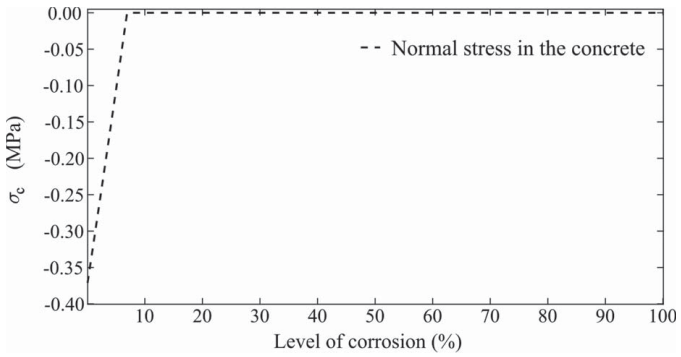

Fig. 17. Variation of the normal stresses in the concrete covering as a function of the corrosion level (C%) for the three different scenarios.

inner tendons. When the total percentage of corrosion (calculated with respect to the initial steel area) is about 55%, the stress in the steel overcomes the ultimate tensile strength (1,700 MPa) and the cable-stay, according to the present hypotheses, collapses under the effect of applied loads (without considering fatigue effects).

In scenario B (Fig. 15), the corrosion proceeds starting from inner tendons. The stress in steel, after the discontinuity around to 7% corrosion, increases gradually and reaches the ultimate limit strength in the outer tendons of around 50%, before the inner tendons are completely corroded. At that point, the area of outer tendons is put equal to zero, and the axial force redistributed to the remaining part of inner tendons. As the resulting normal stress exceeds the tensile strength, the cable-stay collapses immediately.

In scenario C (Fig. 16), it is assumed that corrosion proceeds contemporary in inner and outer tendons. After concrete decompression (at 7% corrosion), the stress in steel tendons increases gradually. At around 47% corrosion, the area of outer tendons is completely eroded, and the stress drops to zero. Analogously to the previous scenario, when the corrosion level approaches 55%, the stress in the inner tendons overcome the tensile strength and the cable-stay collapses.

It is worth noting that a corrosion level between about 50% and 55% is the value obtained also from independent study available in the literature (Calvi et al. 2019), on the basis of complex explicit finite element modeling (FEM) numerical simulations. Furthermore, the described scenarios refer to very critical cross-sections close to the antenna, where the precompression of the concrete covering is particularly ineffective. The same calculation performed at a section at cable-stay mid-span provided 26% corrosion for decompression and about 55% for collapse. At the connection with the deck, the corrosion level for decompression is even higher (43%) but the collapse takes place quite soon after.

Stiffness of the Cable-Stay

Eventually, it is essential to assess the decrease in the cable-stay axial stiffness due to the decompression of concrete along the length of the stay. In fact, if decompression had caused a sensible decrease in the cable-stay stiffness, anomalous deflections and localized damage of the main bridge deck would have been detectable, in contrast to what was observed before of the collapse of Polcevera bridge. In fact, a post hoc analysis for the assessment of possible prefailure bridge deformations (Milillo et al. 2019), based on synthetic aperture radar (SAR) observations, has revealed maximum deflections of the deck lower than about 120–150 mm, although the authors have revealed that the bridge was undergoing an increased magnitude of deformations over time prior to its collapse.

The simple model introduced above provides the unit-length or cross-section stiffness as a function of the level of corrosion. With the axial force diagram from the equation of the elastic catenary being known, it is thus possible to obtain the diagram of axial strains and, by integration along the curvilinear abscissa, the resulting vertical component of the displacement at the cable-stay extremity in correspondence of the bridge deck. It is assumed that corrosion takes place uniformly along the cable-stay length. This hypothesis is conservative in the sense that provides an overestimation of the vertical displacement, with respect to what can be obtained assuming more localized (e.g., pitting corrosion) and likely corrosion patterns.

The origin of the curvilinear coordinate frame is assumed in correspondence to the antenna. Fig. 18 shows the variation of the local axial stiffness with the stay length for increasing corrosion level from 0% up to 35%, with discrete steps of 3.2%. The discontinuity in the stiffness takes place at the boundary between the regions of decompressed and of intact concrete. It can be observed that increasing the corrosion level, the length of the decompressed region increases, whereas its stiffness decreases. This is even more clear from Fig. 19, which shows the evolution of the decompressed region length as a function of the uniform corrosion percentage.

Fig. 20 shows the elongation of the cable-stay due to the axial stiffness decrease, obtained by integration of the axial strain. The magnitude of the stay elongation, and the corresponding vertical displacement becomes appreciable only for uniform corrosion levels above about 30%.

Fatigue Accumulation in the Bridge Stays

Moving Loads and Fatigue Load Spectrum

In general, the fatigue load spectrum can be obtained computing the stress range and the corresponding number of cycles that the structure will withstand during its service life. In particular, the European Standards (CEN 2003) provide five different fatigue load models, which require increasing levels of knowledge about the traffic statistics. Unfortunately, the fatigue model FLM5 could not be adopted, due to the lack of information about registered traffic data during the service life of the Polcevera bridge. Therefore, the fatigue model FLM4, that subdivides the heavy traffic on the basis of a set of five equivalent lorries and disregards the interaction among lorries, is used to assess the stress–amplitude time history. The amplitude of the axial force cycle in the cable-stay owing to the transit of each lorry of a given category is obtained from the influence line of the vertical reaction in point A (due to the unit

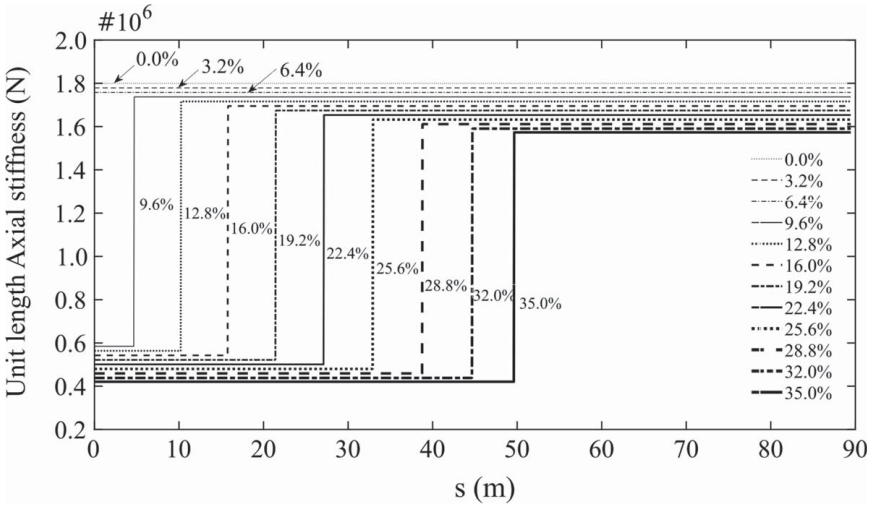

Fig. 18. Variation of axial stiffness of the cable along its length for different corrosion levels.

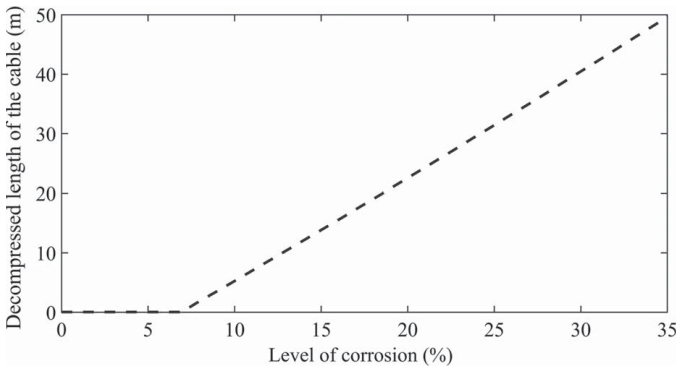

Fig. 19. Decompressed length of the cable versus corrosion level.

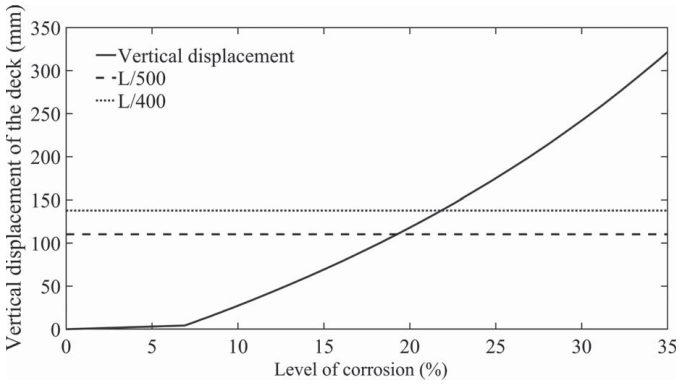

Fig. 20. Vertical displacements of the deck for different corrosion levels.

vertical moving load). Assuming that the lorries travel only on the slow lane, and accounting for the safety distance between lorries, it appears that each heavy vehicle passage corresponds to one main load cycle (CEN 2003). The ratio of the load cycle amplitude to the weight of the lorry, which is equal to about 1.3, corresponds to the difference between the highest peak and the lowest valley values in the influence line, as shown in detail in Invernizzi et al. (2019). Finally, assuming that the heavy truck is entirely supported by the nearby stay, the amplitude of the load cycle in the stay can be obtained projecting the vertical reaction variation at the point A onto the cable. The total number of heavy lorries traffic has been estimated based on a report by Autostrade per l'Italia (MTE 2011). The first reported evidence is that the number of heavy vehicles crossing the bridge has increased by a factor of four since the construction time. The second information is that 2,150,945 lorries have crossed the bridge in both directions during the year 2007. Assuming, for the sake of simplicity, a linear increment in time of the traffic, it is possible to calculate the total number of load cycles. Finally, the relative frequency of each typology of lorries, compared to that of the total traffic, can be assessed according to the European Standard (CEN 2003) indications. The numbers of cycles for each axial load range are summarized in Table 2.

Wöhler's Curve Assessment

The design of new bridges with respect to the fatigue phenomenon can be carried out according to the European Standards (CEN 2006), which basically assume the so-called stress-life approach with a Wöhler's curve that attains an asymptotic fatigue limit when the number of cycles exceeds 10^8 (Nussbaumer et al. 2018). Furthermore, in correspondence of 2×10^6 cycles, Wöhler's curve adopted by EC3 (CEN 2006) shows a change of slope when the transition from the high cycle fatigue (HCF) to the VHCF regime occurs, which varies from 4 to 6 (Sonsino 2007). Note that, although the European Standards define the presence of a horizontal asymptote at 10^8, a further decrease in the fatigue strength has been experimentally observed in the VHCF regime (Bathias and Paris 2004). Moreover, the Wöhler's curve adopted in CEN (2006) refers to the current steel tendons used nowadays in civil constructions. In order to check whether this could be reasonably assumed for the steel strands used for the construction of the Morandi viaduct, we carried out a historical survey of the fatigue strength tests results obtained at the Politecnico di Torino between the mid-1950s and the end of the 1960s on steel tendons. In each collected data sheet, the ultimate tensile strength, the relaxation reduction coefficient, as well as the fatigue life under constant amplitude fatigue loading are reported. Note that, because the tests were carried out at a mean stress of 900 MPa, different from a mean stress of 1,100 and 1,200 MPa currently used, the mean stress correction was performed with the Goodman linear equation (Schijve 2014). The corrected historical data are represented in Fig. 21 versus the Wöhler's curve adopted in CEN (2006), showing a reasonable agreement.

Table 2. Fatigue load spectrum of the stay cable

Type of vehicle	Axial force range (kN)	Number of cycles
1	651.84	15,815,775
2	1010.35	3,953,944
3	1597.01	39,539,438
4	1271.08	11,861,831
5	1466.63	7,907,888

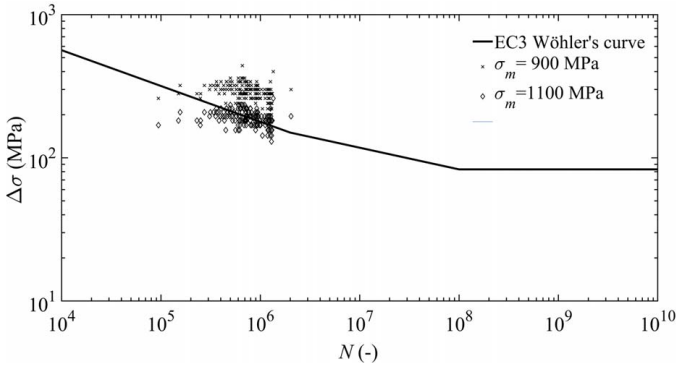

Fig. 21. Comparison between EC3 S–N curve and experimental data from the Politecnico di Torino database.

Unfortunately, in the case of Polcevera bridge, the corrosion of metallic parts developed faster than expected, due to both underestimation of the aggressiveness of the environment and difficult maintenance, so that Wöhler's curve adopted in CEN (2006) must be modified in order to account for the phenomenon of corrosion fatigue.

The term corrosion fatigue refers to the combined action of cyclic loading and corrosive environment. In fact, if an aggressive environment is present during the total life of a structure subjected to fatigue loading, the crack initiation period and crack growth period will decrease enormously due to the synergy of corrosion and fatigue acting together (Stephens et al. 2000). In fact, the repeated loading allows the diffusion of aggressive media between the crack faces toward the crack tip, resulting in an accelerated corrosive action. On the other hand, the corrosion action increases the fatigue damage (Stephens et al. 2000). In more detail, corrosion increases the surface roughness due to the presence of corrosion pits. As a consequence, stress concentration takes place at the root of corrosion pits, which act as cracks nucleation sites accelerating the process of crack initiation at surface flaws (Suresh 2008). In addition, the cyclic loading could determine the rupture of the protective surface of the oxide film, enhancing the electrochemical attack of the aggressive medium at these preferential locations (Suresh 2008). Moreover, corrosion is responsible for various chemical processes, cyclic slips, and rupture mechanisms at the crack tip, which boost the crack propagation rate (Schijve 2014; Lotsberg 2016).

Nakamura and Suzumura (2013) conducted cyclic tests on corroded steel galvanized wire specimens under wet conditions and noted that the fatigue crack propagation is accelerated by the hydrogen produced from the chemical reactions. The same authors observed that corrosion influences the ductility of the galvanized steel wires, whereas the actual ultimate tensile strength does not decrease with the corrosion (Nakamura and Suzumura 2009). In general, corrosion causes a dramatic degradation in fatigue life of steel components, as observed by Li et al. (2012), who carried out fatigue tests on corroded wires used in a cable-stayed bridge in China that had been in service for 18 years. Jiang et al. (2018) observed modifications of Wöhler's curve of corroded steel wires. In the HCF regime, the curve in the bilogarithmic diagram is translated downwards maintaining the same slope. In the VHCF regime, there is a change in the slope of the S–N curve, which increases considerably beyond 2×10^6, if compared with the slopes obtained for noncorroded specimens (Pfennig et al. 2013). In general, corrosion has a more drastic effect in the VHCF regime (Bandara et al. 2015). As a consequence, when fatigue tests are carried out in the range below 10^7 cycles, they may lead to a large overestimation of the corrosion fatigue resistance in the case of a simplistic extrapolation of the curve in the VHCF regime (Perez-Mora et al. 2015). In particular, the most crucial change in the presence of corrosion is the vanishing of the fatigue limit (Nussbaumer et al. 2018).

Note that an analogous modification in Wöhler's curve must be considered if the influence of structural size is considered (Carpinteri and Montagnoli 2019; Montagnoli et al. 2020; Carpinteri et al. 2020).

In the following, for the sake of simplicity, the model proposed in Lotsberg (2016) is used, which considers a linear S–N curve translated rigidly downwards in the HCF regime, without any change in the slope in the VHCF region, according to the experimental data reported in Perez-Mora et al. (2015).

Fatigue Damage Accumulation and Different Collapse Scenarios

Wöhler's curve in European Standards is obtained for constant-amplitude fatigue loading, which means cyclic loading with a constant amplitude and a constant mean load (Schijve 2014). On the other hand, various civil and mechanical structures in service are subjected to variable-amplitude (VA) loading, as in the case of Polcevera bridge. Therefore, because the stress range is not constant, a rule for the damage accumulation must be adopted (CEN 2005, 2006).

The damage increment per load cycle depends not only on the amplitude of the load cycle, but also by the damage caused by preceding cycles (Schijve 2014). Unfortunately, the available information about the traffic is poor, and no measurements were performed on the actual loads' sequence. Therefore, we assumed the Palmgren–Miner rule (Miner 1945), which is a simple linear cumulative fatigue damage rule for fatigue life prediction in the presence of VA loading, that completely disregards the sequence effects of loading cycles (Mayer et al. 2009).

Let us assume that N_i is the number of cycles to failure when the constant stress range $\Delta\sigma_i$ is applied until collapse. If $\Delta\sigma_i$ is a certain applied stress range with the absolute frequency n_i, the partial damage due to each stress range is given by the ratio n_i/N_i. The fatigue failure occurs when the accumulated damage reaches the unity. First, knowing the variation in the axial force of the stay, it is necessary to evaluate the corresponding stress range acting on the material.

According to designer's conception, the precompression of the stays would have guaranteed that the structure had been less prone to the fatigue damage accumulation, because the cyclic loading would have been almost fully supported by the concrete covering, and the stress ranges in the steel elements would have been negligible.

Vice versa, the previous analyses have shown how the decompression of the concrete covering at sections close to the antenna has likely occurred quite soon after the bridge construction. As a consequence, even in correspondence with only one decompressed section, the load cycles were supported by the steel tendons alone, while keeping the rigidity of the entire tie-rod practically unchanged.

Lacking for more detailed information, it is feasible to assume that the corrosion degradation of the steel tendons increased linearly from 0% at the construction time to the collapse critical value due to the combined effect of corrosion and fatigue. Since before 1979 the concrete was likely not decompressed, therefore no

fatigue damage accumulation in the steel tendons took place before that time. Vice versa, as soon as the steel tendons alone began to support the fatigue loads, the fatigue damage accumulated up to the final collapse of the bridge.

It is worth emphasizing that the degradation of the steel tendons must be considered from two different points of view. On one side, corrosion induces fundamental modifications in Wöhler's curve, including the translation downwards of the curve and the disappearance of the horizontal asymptote (Lotsberg 2016). On the other hand, corrosion erodes the steel resisting cross-section, causing an increase in the stress range because of the induced redistribution mechanisms. Therefore, the stress range in the outer and the inner tendons due to each different vehicle category has to be assessed considering the progressive cross-section reduction due to the corrosion, namely:

$$\Delta\sigma_s(C\%, \text{lorry\_cat}) = \frac{\Delta T(\text{lorry\_cat})}{A_s(C\%)} \tag{15}$$

The critical percentage of corrosion, necessary to trigger the collapse of the Polcevera bridge, cannot be obtained explicitly and must be worked out by iterative calculation.

It is worth noting that, even for a certain lorry category, the stress amplitude is not constant with respect to time due to the corrosion cross-section reduction. In addition, the frequency of cycles is not constant with respect to time, due to the increase of heavy lorry traffic. Therefore, the Palmgren–Miner rule must be discretized in time, in order to define time intervals, Δt_i (equal to 1 year), where the stress range, $\Delta\bar{\sigma}_s(t_i)$, and the heavy lorry frequency, $n_i(t_i)$, are approximately constant. Consequently, the fatigue damage accumulation, D, was assessed by using the following expression:

$$D = \sum_i \frac{n_i(\Delta\bar{\sigma}_s(t_i))}{N_i(\Delta\bar{\sigma}_s(t_i))} \tag{16}$$

where $N_i(\Delta\bar{\sigma}_s(t_i))$ is the fatigue life for a constant applied stress range level.

The final level of corrosion, which provides a unit fatigue damage accumulation in the year 2018, is approximately equal to 33% (Fig. 22). It is worth noting that the obtained final corrosion, together with the assumption of linear evolution of corrosion, provides that the corrosion level of 7% would have been reached in 1979, in perfect agreement with the assumption made above for the decompression of concrete starting from the end of the 1970s. In Fig. 23, the five loading cycle amplitudes, corresponding to the typology of the five lorries adopted by FLM4 (Table 2), are represented in the S–N diagram together with the European Standard Wöhler's curve for full cross-section steel tendons (CEN 2006), and the Wöhler's curve for steel in marine environments (Lotsberg 2016). Note that the load cycle amplitude for each category increases due to the above-mentioned reduction in steel cross-section and consequent stress redistribution. Moreover, as far as the mean stress is concerned, note that both Wöhler's curve for intact steel tendons (CEN 2006) and Wöhler's curve for steel in marine environments (Lotsberg 2016) are obtained for values of the mean stress around 1,100 MPa, which is comparable to the stress obtained in the stay strands after concrete decompression.

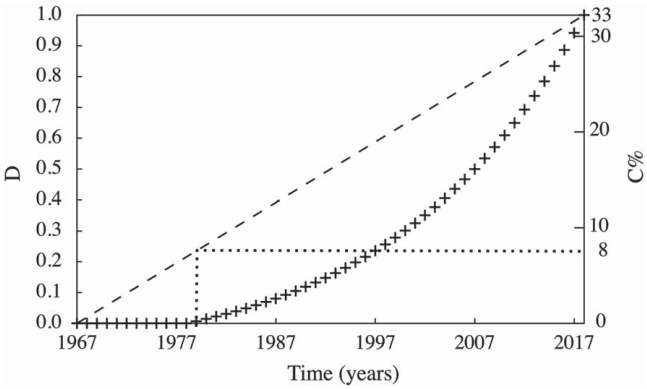

Fig. 22. Palmgren–Miner rule fatigue damage accumulation and linear increment in corrosion up to 33% as a function of time.

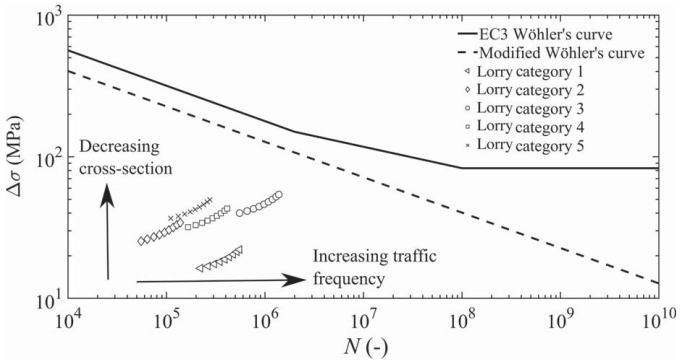

Fig. 23. Application of the Palmgren–Miner rule according to fatigue load spectrum with a corrosion level equal to 33%. Note that, for the sake of clarity, each marker is representative of an almost 6-year time interval.

Conclusions

On August 14, 2018, the pioneering bridge over the Polcevera conceived by Morandi collapsed suddenly. The collapse of the self-standing system 9, which together with the two nearby Gerber beams was rather brittle, lead to the bridge design being blamed for the lack of robustness and structural redundancy (Bazzucchi et al. 2018). On the other hand, thanks to the presence of the Gerber beams, the collapse did not propagate disproportionately to the entire viaduct.

The brittleness of the collapse, as well as the considerable increase in the traffic frequency since the construction time, suggested a careful check with respect to fatigue damage accumulation. In this paper, a detailed quantitative fatigue analysis has been presented, carried out exploiting simplified although effective analytical models, and accounting for the combined effect of fatigue damage accumulation and corrosion. The obtained failure triggering mechanism, due to the brittle failure of one of the cable-stays close to the antenna, is in good agreement with the explicit finite element calculations carried out in order to reproduce the debris configuration after failure (Calvi et al. 2019; Domaneschi et al. 2020). It is worth noting that the level of corrosion needed to trigger the fatigue failure in the critical section is rather low, especially if compared with the corrosion level required to trigger the collapse with respect to static loading only. In particular, the latter is almost twice as high as the corrosion level required for the fatigue failure, regardless of the adopted corrosion scenario. In the presence of aggressive environments, the modification in Wöhler's curve compromises the common concept of fatigue limit, similarly to the case of structural size effects on the fatigue limit (Carpinteri et al. 2020; Carpinteri and Montagnoli 2020; Invernizzi et al. 2021). In fact, if VHCF is approached, even rather limited loading cycles can cause a substantial amount of damage accumulation. The described phenomenon deserves further investigations also in the case of existing steel bridge structures that were built during the 20th century.

Data Availability Statement

All data, models, and code generated or used during the study appear in the published article.

Acknowledgments

This research did not receive any specific grants from funding agencies in the public, commercial, or not-for-profit sectors.

References

Bandara, C., U. Dissanayake, and P. Dissanayake. 2015. "Novel method for developing SN curves for corrosion fatigue damage assessment of steel structures." In *Proc., 6th Int. Conf. on Structural Engineering and Construction Management*, 100–104. Peradeniya, Sri Lanka: University of Peradeniya.

Bathias, C., and P. Paris. 2004. *Gigacycle fatigue in mechanical practice*. New York: Marcel Dekker.

Bazzucchi, F., L. Restuccia, and G. Ferro. 2018. "Considerations over the Italian road bridge infrastructure safety after the Polcevera viaduct collapse: Past errors and future perspectives." *Frat. Integrità Strutt.* 12 (46): 400–421. https://doi.org/10.3221/IGF-ESIS.46.37.

Bonchi, K. 2020. "Ponte morandi, "i cavi erano corrosi": Il messaggio tra gli arrestati conferma la tesi dei periti [Morandi Bridge, "the cables were corroded": The message among the arrested confirms the thesis of the experts]. Accessed September 28, 2021. https://www.genova24.it/2020/11/ponte-morandi-i-cavi-erano-corrosi-il-messaggio-tra-gli-arrestati-conferma-la-tesi-dei-periti-245851.

Calvi, G., M. Moratti, J. O'Reilly, N. Scattarreggia, R. Monteiro, and D. Malomo. 2019. "Once upon a time in Italy: The tale of the Morandi bridge." *Struct. Eng. Int.* 29 (2): 198–217. https://doi.org/10.1080/10168664.2018.1558033.

Carpinteri, A., and F. Montagnoli. 2019. "Scaling and fractality in fatigue crack growth: Implications to Paris' law and Wöhler's curve." *Procedia Struct. Integrity* 14: 957–963. https://doi.org/10.1016/j.prostr.2019.07.077.

Carpinteri, A., and F. Montagnoli. 2020. "Scaling and fractality in subcritical fatigue crack growth: Crack-size effects on Paris' law and fatigue threshold." *Fatigue Fract. Eng. Mater. Struct.* 43 (4): 788–801. https://doi.org/10.1111/ffe.v43.4.

Carpinteri, A., F. Montagnoli, and S. Invernizzi. 2020. "Scaling and fractality in fatigue resistance: Specimen-size effects on Wöhler's curve and fatigue limit." *Fatigue Fract. Eng. Mater. Struct.* 43 (8): 1869–1879. https://doi.org/10.1111/ffe.v43.8.

CEN (European Committee for Standardization). 2003. *Eurocode 1: Actions on structures part 2: Traffic loads on bridges*. EN 1991-2. Brussels, Belgium: CEN.

CEN (European Committee for Standardization). 2005. *Eurocode 3: Design of steel structures: Fatigue strength of steel structures*. EN 1993-1-9. Brussels, Belgium: CEN.

CEN (European Committee for Standardization). 2006. *Eurocode 3: Design of steel structures: Design of structures with tension components made of steel*. EN 1993-1-11. Brussels, Belgium: CEN.

CEN (European Committee for Standardization). 2011. *Eurocode 2: Design of concrete structures - part 1-1: General rules and rules for buildings*. EN 1992-1-1. Brussels, Belgium: CEN.

Domaneschi, M., C. Pellecchia, E. De Iuliis, G. Cimellaro, M. Morgese, A. Khalil, and F. Ansari. 2020. "Collapse analysis of the Polcevera viaduct by the applied element method." *Eng. Struct.* 214 (2): 110659. https://doi.org/10.1016/j.engstruct.2020.110659.

Guardia di Finanza di Genova. 2019. "Ponte morandi: Le immagini inedite della tragedia [Ponte Morandi: The unpublished images of the tragedy]." Youtube accessed October 1, 2019. https://www.youtube.com/watch?v=a-LfXohbn0U.

Invernizzi, S., F. Montagnoli, and A. Carpinteri. 2019. "Fatigue assessment of the collapsed xxth century cable-stayed Polcevera bridge in Genoa." *Procedia Struct. Integrity* 18: 237–244. https://doi.org/10.1016/j.prostr.2019.08.159.

Invernizzi, S., F. Montagnoli, and A. Carpinteri. 2020a. "The collapse of the Morandi's bridge: Remarks about fatigue and corrosion." In *Proc., IABSE Symp., Wroclaw 2020: Synergy of Culture and Civil Engineering – History and Challenges*, edited by J. Bień, J. Biliszczuk, P. Hawryszków, M. Hildebrand, M. Knawa-Hawryszków, and K. Sadowski, 1040–1047. Zurich, Switzerland: IABSE.

Invernizzi, S., F. Montagnoli, and A. Carpinteri. 2020b. "Corrosion fatigue investigation on the possible collapse reasons of Polcevera bridge in Genoa." In *Proc., XXIV AIMETA Conf. 2019*. Lecture Notes in Mechanical Engineering, edited by A. Carcaterra, A. Paolone, and G. Graziani, 151–159. Berlin: Springer.

Invernizzi, S., F. Montagnoli, and A. Carpinteri. 2021. "Experimental evidence of specimen-size effects on EN-AW6082 aluminum alloy in VHCF regime." *Appl. Sci.* 11 (9): 4272. https://doi.org/10.3390/app11094272.

Irwine, M. 1981. *Cable structures*. Cambridge, UK: The MIT Press.

Jiang, C., C. Wu, and X. Jiang. 2018. "Experimental study on fatigue performance of corroded high-strength steel wires used in bridges." *Constr. Build. Mater.* 187 (3): 681–690. https://doi.org/10.1016/j.conbuildmat.2018.07.249.

Li, H., C. Lan, Y. Ju, and D. S. Li. 2012. "Experimental and numerical study of the fatigue properties of corroded parallel wire cables." *J. Bridge Eng.* 17 (2): 211–220. https://doi.org/10.1061/(ASCE)BE.1943-5592.0000235.

Lotsberg, I. 2016. *Fatigue design of marine structures*. Cambridge, UK: Cambridge University Press.

Mayer, H., C. Ede, and J. Allison. 2009. "Influence of cyclic loads below endurance limit or threshold stress intensity on fatigue damage in cast aluminium alloy 319-T7." *Int. J. Fatigue* 27 (2): 129–141. https://doi.org/10.1016/j.ijfatigue.2004.06.004.

Milillo, P., G. Giardina, D. Perissin, G. Milillo, A. Coletta, and C. Terranova. 2019. "Pre-collapse space geodetic observations of critical infrastructure: The morandi bridge, Genoa, Italy." *Remote Sens.* 11 (12): 1–14. https://doi.org/10.3390/rs11121403.

Miner, M. 1945. "Cumulative damage in fatigue." *J. Appl. Mech.* 12 (3): A159–A164. https://doi.org/10.1115/1.4009458.

Ministero delle infrastrutture e della mobilità sostenibili (MIT). 2018. *Relazione della commissione ispettiva mit*. Rep. no. Italian Ministry of Infrastructure. Accessed August 18, 2021. https://www.mit.gov.it/comunicazione/news/ponte-morandi-online-la-relazione-della-commissione-ispettiva-mit.

Montagnoli, F., S. Invernizzi, and A. Carpinteri. 2020. "Fractality and size effect in fatigue damage accumulation: Comparison between Paris and Wöhler perspectives." In *Proc., XXIV AIMETA Conf. 2019*. Lecture Notes in Mechanical Engineering, edited by A. Carcaterra and G. Paolone, A. and Graziani, 188–196. Berlin: Springer.

Morandi, R. 1967. "Il viadotto sul polcevera per l'autostrada Genova-Savona." *L'Industria Italiana del Cemento* 12 (200): 849–872.

Morandi, R. 1968. "Viaducto sobre el polcevera en genova italia, informes de la construccion." *Inf. Constr.* 21 (200): 57–88. https://doi.org/10.3989/ic.1968.v21.i200.

Morandi, R. 1979. "The long-term behaviour of viaducts subjected to heavy traffic and situated in an aggressive environment: The viaduct on the Polcevera in Genoa." *IABSE Reports of the Working Commissions*, 32, 170–180.

Ministero della Transizione Ecologica (MTE). 2011. *Relazione generale sinottica, 2011*. Rep. No. Ministero dell'Ambiente e della Tutela del Territorio e del Mare. Accessed August 18, 2021. https://va.minambiente.it/it-IT/Oggetti/MetadatoDocumento/22144.

Nakamura, S., and K. Suzumura. 2009. "Hydrogen embrittlement and corrosion fatigue of corroded bridge wires." *J. Constr. Steel Res.* 65 (2): 269–277. https://doi.org/10.1016/j.jcsr.2008.03.022.

Nakamura, S., and K. Suzumura. 2013. "Experimental study on fatigue strength of corroded bridge wires." *J. Bridge Eng.* 18 (3): 200–209. https://doi.org/10.1061/(ASCE)BE.1943-5592.0000366.

Nussbaumer, A., L. Borges, and L. Davaine. 2018. *Fatigue design of steel and composite structures: Eurocode 3: Design of steel structures, Part 1-9: Fatigue; Eurocode 4: Design of composite steel and concrete structures*. 2nd ed. Translated by D. B. Steinman. Berlin: Wilhelm Ernst & Sohn Verlag für Architektur und technische Wissenschaften GmbH & Co. KG.

Perez-Mora, R., T. Palin-Luc, C. Bathias, and P. Paris. 2015. "Very high cycle fatigue of a high strength steel under sea water corrosion: A strong

corrosion and mechanical damage coupling." *Int. J. Fatigue* 74: 156–165. https://doi.org/10.1016/j.ijfatigue.2015.01.004.
Pfennig, A., M. Wolf, R. Wieganda, A. Kranzmannb, and C. Borkb. 2013. "Corrosion fatigue behavior and S-N-curve of X46Cr13 exposed to CCS-environment obtained from laboratory in-situ-experiments." *Energy Procedia* 37 (2): 5764–5772. https://doi.org/10.1016/j.egypro.2013.06.499.
Schijve, J. 2014. *Fatigue of structures and materials*. Berlin: Springer.
Sonsino, C. 2007. "Course of SN-curves especially in the high-cycle fatigue regime with regard to component design and safety." *Int. J. Fatigue* 29 (12): 2246–2258. https://doi.org/10.1016/j.ijfatigue.2006.11.015.
Stephens, R. I., A. Fatemi, R. R. Stephens, and H. O. Fuchs. 2000. *Metal fatigue in engineering*. Hoboken, NJ: Wiley.
Suresh, S. 2008. *Fatigue of materials*. Cambridge, UK: Cambridge University Press.